Nanotechnology **20** (2009) 305705 (8pp) doi:10.1088/0957-4484/20/30/305705

Evolution of metastable phases in silicon during nanoindentation: mechanism analysis and experimental verification

K Mylvaganam[1], L C Zhang[2,5], P Eyben[3], J Mody[4] and W Vandervorst[3,4]

[1] Centre for Advanced Materials Technology, The University of Sydney, NSW 2006, Australia
[2] School of Mechanical and Manufacturing Engineering, The University of New South Wales, NSW 2052, Australia
[3] IMEC, Kapeldreef 75, B-3001 Leuven, Belgium
[4] KU Leuven, Electrical Engineering Department, INSYS, Kasteelpark Arenberg 10, B-3001 Leuven, Belgium

E-mail: k.mylvaganam@usyd.edu.au, Liangchi.zhang@unsw.edu.au, eyben@imec.be, jamody@imec.be and vdvorst@imec.be

Received 14 April 2009, in final form 26 May 2009
Published 8 July 2009
Online at stacks.iop.org/Nano/20/305705

Abstract

This paper explores the evolution mechanisms of metastable phases during the nanoindentation on monocrystalline silicon. Both the molecular dynamics (MD) and the *in situ* scanning spreading resistance microscopy (SSRM) analyses were carried out on Si(100) orientation, and for the first time, experimental verification was achieved quantitatively at the same nanoscopic scale. It was found that under equivalent indentation loads, the MD prediction agrees extremely well with the result experimentally measured using SSRM, in terms of the depth of the residual indentation marks and the onset, evolution and dimension variation of the metastable phases, such as β-Sn. A new six-coordinated silicon phase, Si-XIII, transformed directly from Si-I was discovered. The investigation showed that there is a critical size of contact between the indenter and silicon, beyond which a crystal particle of distorted diamond structure will emerge in between the indenter and the amorphous phase upon unloading.

(Some figures in this article are in colour only in the electronic version)

1. Introduction

The complexity of phase transformations in silicon is well known. Using a low-energy electron microscopy, Hannon *et al* [1] showed that the dynamics of surface phase transformation is different from the bulk systems. During nano/microindentation, a series of investigations, both theoretical [2–6] and experimental [7–12], has identified various stable and non-stable phases. Evolutions of some of those phases have been explained by monitoring the positions of atoms in the MD simulations of nanoindentation [3]. However, direct quantitative correlation between theoretical and experimental indentation studies has never been established due to their difference in dimensional scales. The magnitude of the maximum indentation load in an MD simulation is often several orders lower than that in an experiment. The attempt of multi-scale simulations [13] based on the concept of local quasi-continuum has failed to reach a quantitative agreement with experiment.

The metastable phase of silicon, β-Sn (or Si-II), is an intermediate phase formed on loading [3], which diminishes during unloading. Thus unlike the R8/BC8 phases of Si, which can be identified after an indentation test using high resolution transmission electron microscopy (HRTEM) [10, 12] and Raman analysis [14], it is difficult to directly identify or detect β-Sn during or after an indentation. When monocrystalline Si of diamond structure (Si-I) was loaded in a diamond anvil cell under a sufficiently high hydrostatic stress, it was reported that a phase transformation from the cubic diamond Si to the

[5] Author to whom any correspondence should be addressed.

 © 2009 IOP Publishing Ltd Printed in the UK

β-Sn structure took place associated with a volume reduction of about 20% [7]. This was coincident with the discontinuity observed in many load–displacement curves of indentations, called 'pop-in'. Then without a solid verification, the location of a pop-in was regarded as a signal of the onset of the β-Sn phase transition by many researchers. As a result, in the interpretation of many phenomena in nanoindentation tests, the formation of the metastable β-Sn phase during loading has often been assumed. This is inappropriate and inaccurate as has been pointed out recently [15], but there is not a direct experimental evidence of the emergence of β-Sn in indenting Si-I apart from the theoretical predictions by the molecular dynamics analysis [3, 4].

In situ characterization techniques are attractive approaches to study the phase transformations. Park *et al* [16] reported a study using simultaneous topographic and force measurements with a conductive cantilever in an AFM system for a Si sample patterned with n, p regions. Ruffell *et al* [17] presented an *in situ* electrical measurement technique for the investigation of nanoindentation in silicon using a Hysitron Triboindenter. However, sub-nanometer spatial resolution cannot be achieved in their techniques. Scanning spreading resistance microscopy (SSRM) is an electrical characterization technique based on AFM, which is often used to probe the two-dimensional active dopant distribution in semiconductor devices and has been widely accepted for the characterization of silicon devices as well as other semiconductor materials [18]. It has been demonstrated that a small effective radius can be achieved with a full diamond tip in its single scan mode that results in an enhanced spatial resolution of less than 3 nm [19, 20]. Recent measurements in high vacuum (10^{-5} Torr) have reported a sub-nanometer spatial resolution on test structure. It is then highly possible that an *in situ* detection of β-Sn at the same spatial resolution of an MD simulation can be realized by measuring the variation of electrical conductivity of a Si-I specimen under indentation using the SSRM technique. This is because β-Sn is a metallic phase and its electrical conductivity is higher than that of the Si-I phase. If an *in situ* measurement detects a fall in electrical resistivity during loading, then it can be considered as the emergence of β-Sn.

This paper aims to verify the metastable β-Sn phase during the nanoindentation of monocrystalline silicon by comparing directly the MD analysis with SSRM measurement. The scale effect of contact size on the phase transformations will be discussed.

2. Molecular dynamics modeling and SSRM measurement

The MD was used to simulate the nanoindentation experiment on (100) silicon sample using a diamond tip. Hemispherical rigid diamond tips of radius 5, 7.5 and 10 nm that are similar in size to the AFM diamond tips of the SSRM measurements were used as the indenters. To avoid the boundary effect, large silicon samples of dimensions $21.72 \times 21.72 \times 9.77$ nm^3 and $24.44 \times 24.44 \times 11.95$ nm^3 were used in the MD modeling. To make sure that a phase observed is not due to the size effect of the silicon sample, indentation simulations with 7.5 nm tip were done on both samples. Thermostat atoms and boundary atoms were arranged to surround the Newtonian atoms of silicon to ensure a reasonable outward heat conduction and to eliminate the rigid body motion [2, 3]. The velocities of atoms in the initial model follow the Maxwell distribution. Interactions among silicon atoms were described by Tersoff potential [21, 22] and those among silicon and diamond atoms were described by a modified Morse potential, as explained elsewhere [2, 3]. The tip of the indenter was placed 5 Å above the surface of the silicon workpiece and moved towards the workpiece by 0.001 Å per time step of 2.5 fs at a constant temperature of 300 K. In a conventional study of indentation, the indentation depth is the penetration of the indenter measured from the surface of the workpiece. However, on the atomic scale, a definite surface does not exist. To resolve this, it is assumed that the surfaces of the indenter and the workpiece are defined by the envelopes at the theoretical radii of their surface atoms. In this way, the indentation depth becomes consistent with the conventional definition.

To make sure that a phase observed in a simulation is stable under a specific stress level of interest, the indenter in this simulation at this specific stress level (in other words, the position of the indenter at the specific time) was kept unchanged for 37 500 fs.

A sketch of the experimental setup of the SSRM is shown in figure 1, where a diamond AFM probe was indenting into a lowly doped n-type (100) silicon sample having a resistivity of 42 Ω cm, while a d.c. bias is applied between a back contact on the back side of the sample and the tip to realize a stable electrical contact. The resulting current is measured using a logarithmic current amplifier (10 pA–0.1 mA). The applied indentation force is extracted by fixing the spring constant of the probe (5 N m^{-1}). The measurements were made (i) in air and (ii) in N_2 glove-box environment. In the N_2 environment, six different indentations were carried out for load varying between 4.3 and 0.7 μN and the penetration depths were recorded. On applying a voltage, the tip cantilever bending, which is then converted to the force, and the current flow from the tip to the back side of the sample were measured.

In the SSRM indentation experiment, the exact radius of the diamond tip could not be exactly detected *in situ*, but our HRTEM (high resolution transmission electron microscopy) inspections showed that the tip radius at the bottom that would be in contact with the sample was typically between 5 and 10 nm as shown in figure 2. Hence in our MD analysis, three different indenter tips (5, 7.5 and 10 nm) within this range were used for the theoretical modeling, which, on the other hand, could show the scale effect of the indenter dimension if any.

3. Results and discussion

3.1. MD analysis of the microstructural changes

To an indentation depth of 4.0 nm, the indentations into the silicon (100) specimens with diamond tips of radii 5, 7.5 and 10 nm resulted in the maximum loads of 2.5, 3.4 and 4.1 μN,

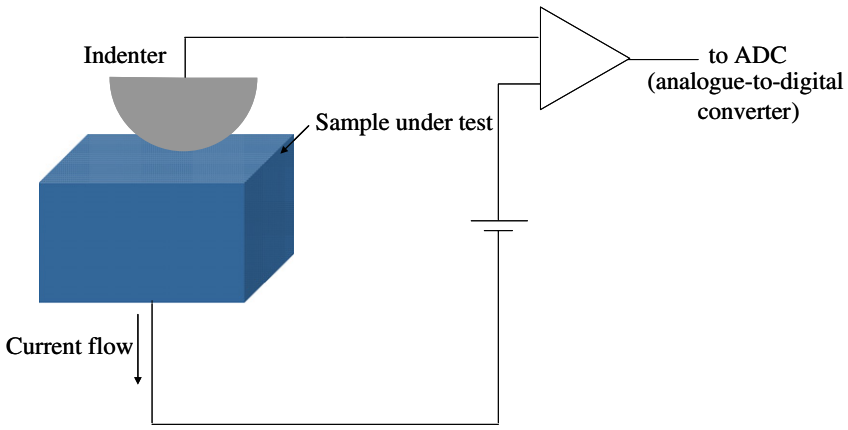


Figure 1. Experimental setup of the indenter and the sample.

respectively. Figure 3 shows the cross-sectional views of the deformed silicon specimens at this depth of indentation. When the indenter radius is small, e.g., 5 nm as in the case in figure 3(a) and the results reported in [3], a volume of β-Sn (six-coordinated atoms, with four bonds of length ∼2.43 Å and two bonds of length ∼2.585 Å, form a crystal structure with lattice parameters $a = 4.684$ Å and $c = 2.585$ Å), as circled, appears around the central axis of the deformation zone and this volume of β-Sn is almost in direct contact with the indenter tip. With the larger indenters, figures 3(b) and (c), it is evident that the orientations of the atoms in regions A and B have become different from the original Si-I. Those in region A are β-Sn, but those in region B are not although they are six-coordinated. Both regions A and B are surrounded by five-coordinated atoms as shown in figure 3(b) in white. The variation of the atomic coordination numbers during the indentation process is shown in figure 4. The number of six-coordinated atoms increased rapidly around an indentation depth of about 2.05 nm. However, unlike the case with a smaller indenter, a larger indenter tends to create the β-Sn phase at a greater distance below the indenter tip. Between region A and the indenter surface, in addition to the five-coordinated atoms (white) mentioned previously, there also exist diamond-like crystalline patches. These are similar to the observation by Kim and Oh [5] in their MD simulations using an indenter of 11 nm in radius.

To explore more clearly the atomic structure of the material in region B, let us observe the details through a top down view of all the six-coordinated atoms in region B as shown in figure 5 (indenter radius $= 7.5$ nm; indentation depth $= 4.0$ nm). It can be clearly seen that the atoms in region B, although six-coordinated, are not β-Sn as those in region A (the central part circled). However, these atoms maintain a crystalline order with their atomic bond details shown in figure 6. This type of six-coordinated crystalline Si has never been discovered or defined before. For the convenience of discussion, let us call this the Si-XIII phase to distinguish it from the other twelve silicon phases already defined in the literature [23]. To find out the formation mechanisms of Si-XIII, we monitored the spatial coordinate variations of some atoms in region B during the whole indentation loading process. This examination shows that the Si-XIII phase in region B is formed directly from the diamond cubic silicon atoms, Si-I, and is initiated after the formation of the β-Sn phase in region A.

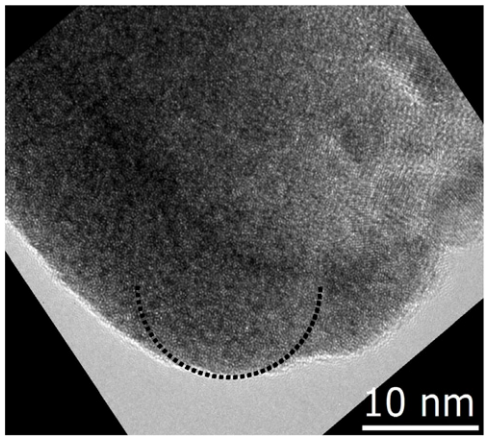


Figure 2. HRTEM view of a fresh SSRM diamond tip. A broad radius of curvature of the tip apex (typically between 5 and 10 nm) can be observed.

Upon unloading, the β-Sn phase in region A loses its crystalline order and changes to amorphous silicon. However, the Si-XIII phase in region B almost maintains its spatial occupation in the deformation zone during the initial period of unloading when the β-Sn phase transforms to the amorphous. Then part of the Si-XIII changes into amorphous phase and the rest returns to the original Si-I structure of the monocrystalline silicon, according to our detailed label identification of the Si-XIII atoms.

As mentioned before, under a larger indenter there exist diamond-like crystalline patches between region A and the tip of indenter, because the atoms in these patches were four-coordinated but distorted and had a short interlayer distance. Upon unloading, these patches grow to a bigger crystalline marked as region C in figure 7. This indicates that on releasing the stresses, some five-coordinated atoms (the white ones in figure 3(b)) surrounding the patches turn to the diamond-like crystalline phase, probably due to the nucleation of these

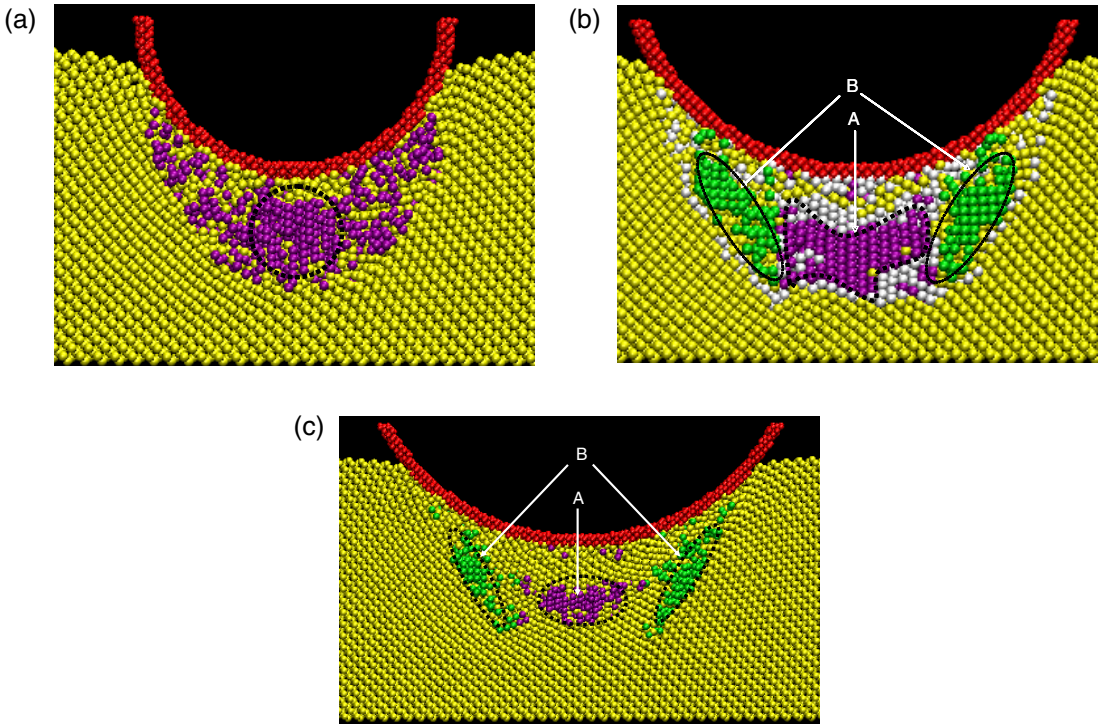


Figure 3. A portion of the cross-sectional view of the atomic positions on indenting with a (a) 5.0 nm, (b) 7.5 nm (c) 10.0 nm radius tips at a maximum indentation depth of 4.0 nm (purple (region A) and green (region B) spheres represent the six-coordinated atoms and white spheres represent the five-coordinated atoms).

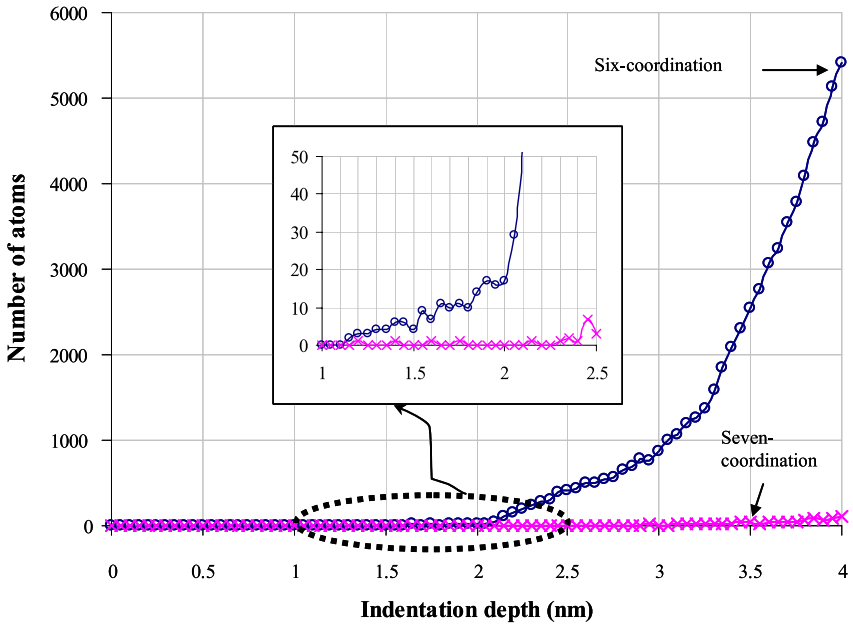


Figure 4. Variation of the number of highly coordinated atoms with tool displacement on loading.

crystalline patches. An atomic lattice structure analysis shows, figure 8, that the material in region C has a distorted diamond structure (DDS) in both bond lengths and angles. However, this is clearly not a R8 or BC8 because no second neighbor in the structure has been identified with the bond length of about 3.5 Å. The distortion could be caused by the residual stresses in the specimen. To the best of our knowledge, such a DDS occupied zone (region C) has never been reported in previous studies although diamond-like R8/BC8 phases were discovered in a similar location of an indentation-induced deformation zone when a larger indenter was used at a higher load [11]. This may indicate that the DDS phase in region C identified above reflects the effect of the indentation scale, because under a smaller indenter region C does not appear at all, while under

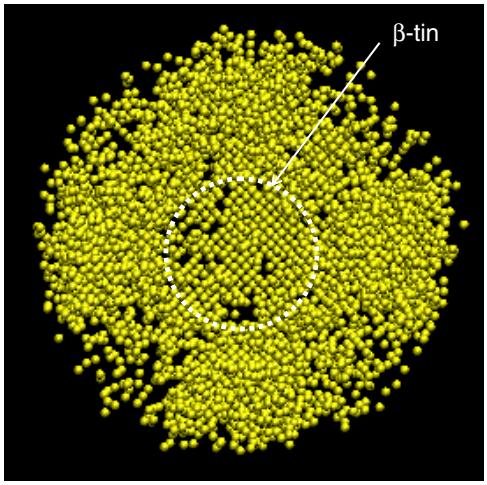


Figure 5. All the six-coordinated atoms at the maximum indentation—top down view.

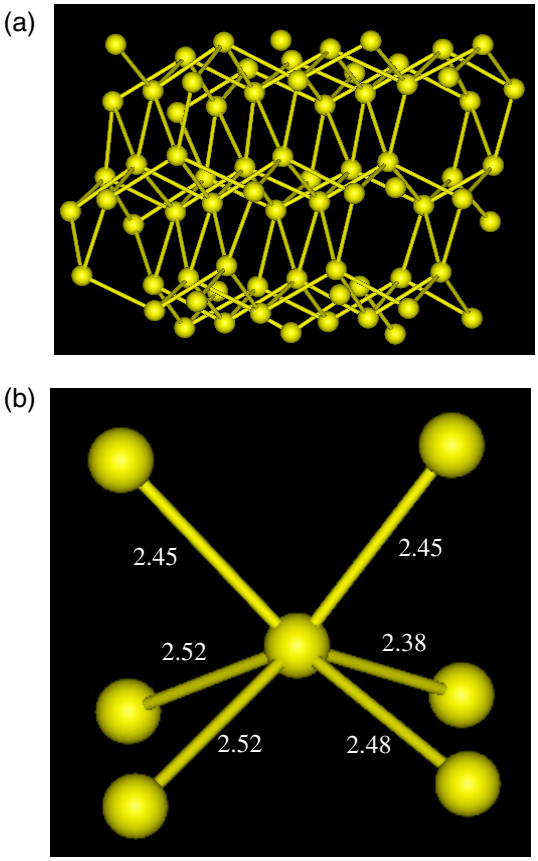


Figure 6. (a) A portion of the atoms in region B showing its crystal structure. (b) Structure of one of the atoms in region B, where the bond lengths are shown in Å.

a larger indenter, R8/BC8 takes place. The DDS phase can be the intermediate structure generated towards the emergence of R8/BC8 at a larger indentation scale.

In summary, we have shown that the deformation of silicon during loading depends on the size of the indenter tip. With the indenter of radius 5 nm, the microstructural evolution

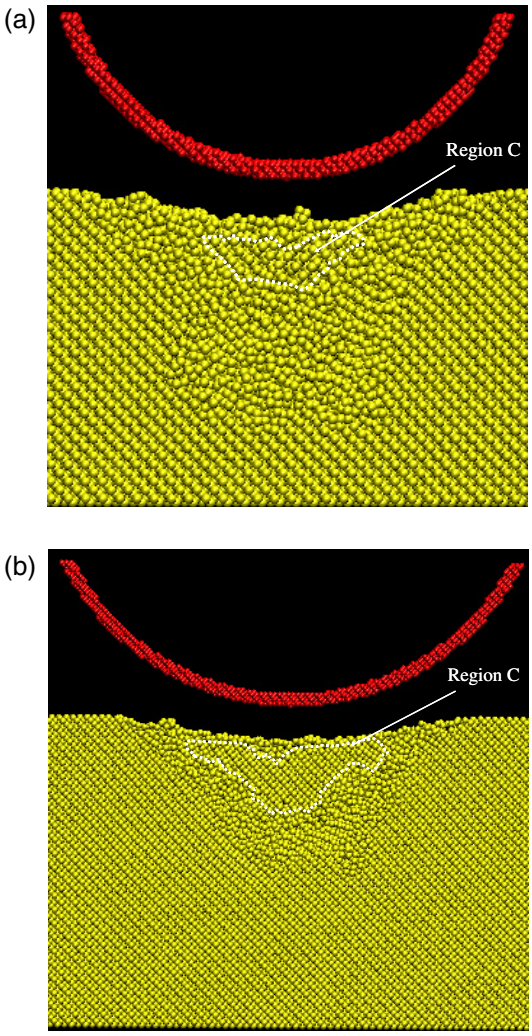


Figure 7. A portion of the cross-sectional view of the atomic positions on unloading when using (a) 7.5 nm and (b) 10.0 nm indenter.

during loading and unloading is the same as that under a much smaller indenter of radius 2.14 nm [1, 2], characterized by the formation of β-Sn in region A mostly directly beneath the indenter surface. There is no noticeable scale effect of indenter size up to a radius of 5 nm. When the indenter size increases further, as shown by figures 3(b) and (c), Si-XIII emerges in region B and small patches of a diamond-like cubic crystalline phase appears in between the indenter and the β-Sn occupied region A. These diamond-like patches will eventually grow up to a larger DDS particle in region C upon complete unloading.

3.2. Experimental verification

As we highlighted earlier, the β-Sn phase caused by mechanical loading is critical to the development of damage-free machining technologies [24]. This phase diminishes during unloading and its emergence and evolution cannot be explored by any experimental means after an indentation test. On the other hand, the magnitude of indentation load and the radius of an indenter in a test are much bigger than those in an

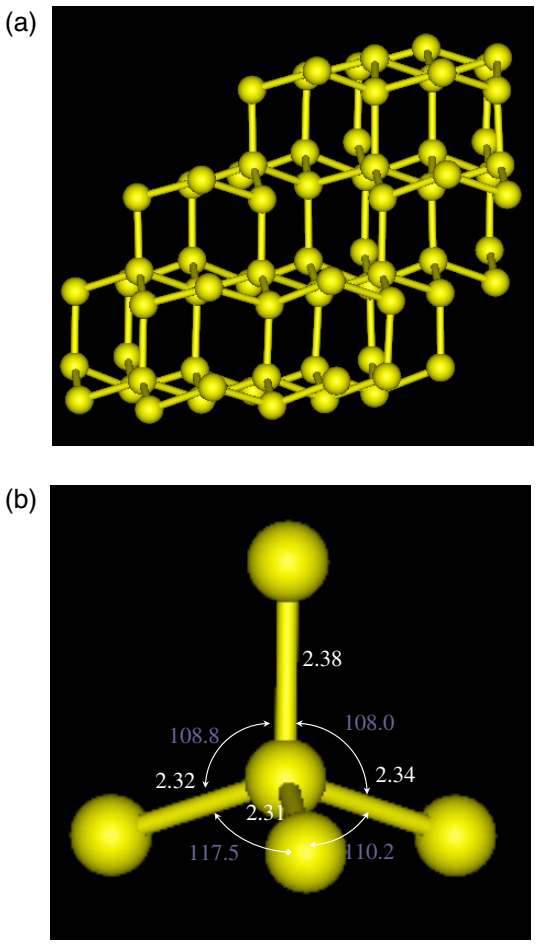


Figure 8. (a) A portion of the atoms in region C. (b) Structure of one of the atoms where the bond lengths are shown in Å and the bond angles are shown in degrees.

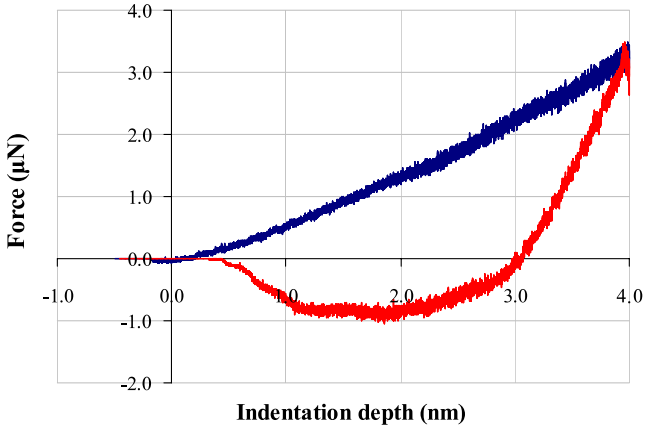


Figure 9. Nanoindentation MD simulation load–displacement curve (tip radius = 7.5 nm).

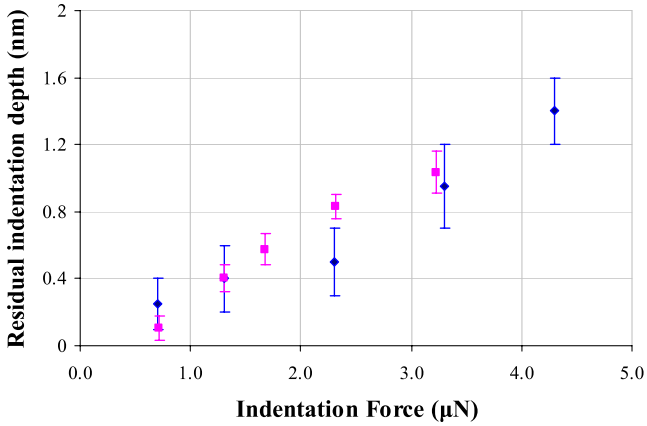


Figure 10. Comparison of SSRM (tapping mode) and MD simulation indentation force—depth results (points in blue color (◆) are SSRM results and in pink color (■) are MD results).

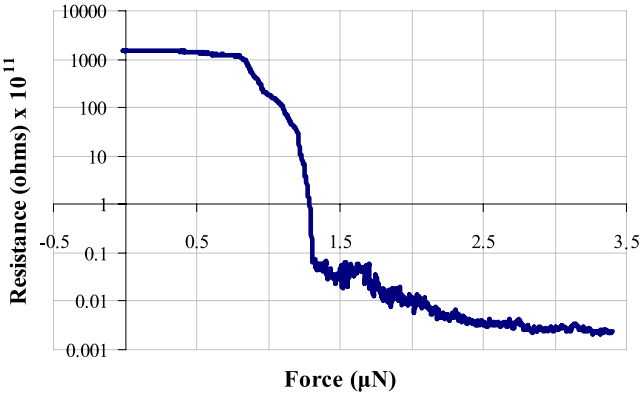


Figure 11. SSRM resistance–force curve.

MD analysis. Hence, the β-Sn phase has never been confirmed directly experimentally. Using the SSRM detailed in section 2, we are now able to provide more direct evidence in relation to the β-Sn phase by comparing the MD predictions and the *in situ* experimental measurement with a similar radius tip to the MD simulations (figure 2). In the following, we will focus on the comparison of the MD results from the indenter of radius 7.5 nm.

Figure 9 is the load–displacement (or indentation depth) curve of a complete nanoindentation from the MD simulation. It shows that at the maximum indentation depth of 4 nm, the indentation force is 3.4 μN. The maximum indentation force from the experimental measurement was about 3.3 μN, which is very close to that from the MD simulation. Figure 10 compares the depths of the residual indentation mark from MD and SSRM indentation (in an inert environment with N_2). The comparison demonstrates that they are in excellent agreement quantitatively. All these mean that we can reasonably compare the microstructural changes revealed by the MD against the experimental measurement in such an indentation process.

In the SSRM measurement during indentation, the current flows through the following resistances: (1) resistance of the tip, (2) the tip–Si contact, (3) the resistance of phase transformed material and (4) the resistance of the rest of Si sample. Of these, contributions to (1), (2) and (4) would be present as soon as the tip comes into contact with the sample. Hence the drop in resistance during indentation could be correlated to the phase transformed material. Figure 11, shows that at the initial stage of indentation loading the electrical

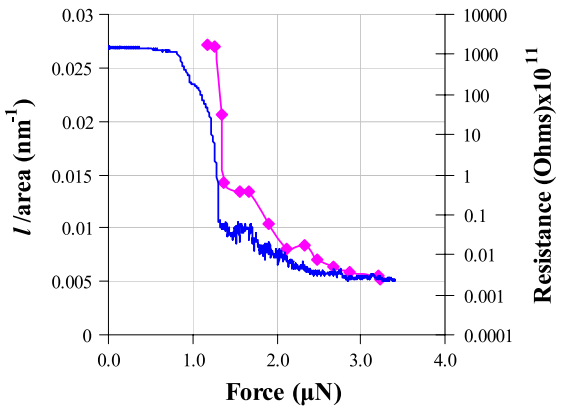


Figure 12. Resistance–force variation—comparison of SSRM (blue) and MD (pink ◆) results.

resistance, R, keeps a constant corresponding to that of Si-I. When the indentation force reaches about 0.824 μN, R suddenly drops until the force reaches about 1.335 μN. This sudden variation in R means that a microstructural change, or in other words a phase transformation, must have taken place in this period and the new phase must have a much lower R compared with that of Si-I such that the overall R measured by the SSRM changes dramatically. Our MD simulation, figure 4, shows that the six-coordinated Si starts to form at the indentation depth of about 1.2 nm, corresponding to the indentation force of about 0.75 μN according to figure 9. After that the β-Sn and Si-XIII phases (six-coordinated) grow rapidly. As has been well established, these six-coordinated phases of silicon are metallic in nature due to a small gap between valence band and conductance band that allows jumping of electrons. Thus their rapid growth reduces the electrical resistance as the experiment shows. We understand that the number of six-coordinated atoms is related to the total atomic pocket volume of the β-Sn and Si-XIII phases shown in figure 3(b), and that the electrical resistance R is determined by $R = \rho(l/A)$ where ρ is the specific resistance, l is the length and A is the cross-sectional area of the β-Sn and Si-XIII pocket. Figure 12 shows the variation of (l/A) with the indentation force (MD result) and the change of the experimentally measured R (logarithmic scale) with the force. They show excellent agreement in terms of the effect of the β-Sn and Si-XIII growth on the sudden drop of R. The above comparison clearly confirms the emergence of β-Sn during nanoindentation loading.

4. Conclusions

Based on the analysis and discussion above, we can come up with the following main conclusions:

(1) We have, for the first time, provided the most direct experimental evidence at the same nanoscopic scale as the molecular dynamics simulation that some metastable phases during the nanoindentation on monocrystalline silicon, including β-Sn, do appear.

(2) Based on our MD simulations, we have discovered a new six-coordinated metastable phase of silicon, Si-XIII, which forms aside the β-Sn zone but does not emerge under a small indenter. We also discovered that under a larger indenter, small patches of a diamond-like cubic crystalline phase can appear in between the indenter and the β-Sn occupied region. Upon complete unloading, these patches will form a larger particle with a distorted diamond-like structure.

Acknowledgments

The authors KM and LCZ thank the Australian Research Council for its continuous financial support. This work was also supported by the Australian partnership for advanced computing.

References

[1] Hannon J B, Hibino H, Bartelt N C, Swartzentruber B S, Ogino T and Kellogg G L 2000 Dynamics of the silicon (111) surface phase transition *Nature* **405** 552–4
[2] Zhang L C and Tanaka H 1999 On the mechanics and physics in the nano-indentation of silicon monocrystals *JSME Int. J.* A **42** 546–59
[3] Cheong W C D and Zhang L C 2000 Molecular dynamics simulation of phase transformations in silicon monocrystals due to nano indentation *Nanotechnology* **11** 173
[4] Cheong W C D and Zhang L C 2000 Effect of repeated nano-indentations on the deformation in monocrystalline silicon *J. Mater. Sci. Lett.* **19** 439–42
[5] Kim D E and Oh S I 2006 Atomistic simulation of structural phase transformations in monocrystalline silicon induced by nanoindentaion *Nanotechnology* **17** 2259–65
[6] Lin Y-H, Jian S-R, Lai Y-S and Yang P-F 2008 Molecular dynamics simualtion of nanoindentation-induced mechanical deformation and phase transformation in monocrystalline silicon *Nanoscale Res. Lett.* **3** 71–5
[7] Hu J Z, Merkle L D, Menoni C S and Spain I L 1986 Crystal data for high-pressure phases of silicon *Phys. Rev.* B **34** 4679–84
[8] McMahon M I, Nelmes R J, Wright N G and Allan D R 1994 Pressure dependence of the *Imma* phase of silicon *Phys. Rev.* B **50** 739–43
[9] Hanfland M, Schwarz U, Syassen K and Takemura K 1999 Crystalstructure of the high-pressure phase silicon V *Phys. Rev. Lett.* **82** 1197–200
[10] Zarudi I, Zhang L C, Zou J and Vodenitcharova T 2004 The R8-BC8 phases and crystal growth in monocrystalline silicon under microindentation with a spherical indenter *J. Mater. Res.* **19** 332–7
[11] Zarudi I and Zhang L C 1999 Structure changes in mono-crystalline silicon subjected to indentation—experimental findings *Tribol. Int.* **32** 701–12
[12] Zarudi I, Zou J and Zhang L C 2003 Microstructures of phases in indented silicon: a high resolution characterization *Appl. Phys. Lett.* **82** 874–6
[13] Smith G S, Tadmor E B and Kaxiras E 2000 Multiscale simulation of loading and electrical resistance in silicon nanoindentation *Phys. Rev. Lett.* **84** 1260–3
[14] Gogotsi Y, Baek C and Kirscht F 1999 Raman microspectroscopy study of processing-induced phase transformations and residual stress in silicon *Semicond. Sci. Technol.* **14** 936–44
[15] Chang L and Zhang L 2009 Mechanical behavior characterisation of silicon and effect of loading rate on

pop-in: a nanoindentation study under ultra-low loads *Mater. Sci. Eng.* A **506** 125–9
[16] Park J Y, Phaneuf R J, Ogletree D F and Salmeron M 2005 Direct measurement of froces during scanning tunneling microscopy imaging of silicon pn junctions *Appl. Phys. Lett.* **86** 172105
[17] Ruffell S, Bradby J E and Williams J S 2007 An *in situ* electrical measurement technique via a conducting diamond tip for nanoindentation in silicon *J. Mater. Res.* **22** 578–86
[18] Eyben P, Vandervorst W, Alvarez D, Xu M and Fouchier M 2007 *SPM: Electrical and Electromechanical Phenomena at the Nanoscale* (Berlin: Springer)
[19] Álvarez D, Hartwich J, Fouchier M, Eyben P and Vandervorst W 2003 Sub-5 nm-spatial resolution in scanning spreading resistance microscopy using full-diamond tips *Appl. Phys. Lett.* **82** 1724
[20] Eyben P, Degryse D and Vandervorst W 2005 On the spatialresolution of scanning spreading resistance microscopy: experimental assessment and electro-mechanical modeling *Characterization and Metrology for ULSI Technology* (Leuven: AIP) pp 264–9
[21] Tersoff J 1986 New empirical model for the structural prpoperties of silicon *Phys. Rev. Lett.* **56** 632
[22] Tersoff J 1989 Modeling solid-state chemistry: interatomic potentials for multicomponent systems *Phys. Rev.* B **39** 5566
[23] Zhang L C and Zarudi I 2001 Towards a deeper understanding of plastic deformation in mono-crystalline silicon *Int. J. Mech. Sci.* **43** 1985–96
[24] Biddut A Q, Zhang L C, Ali Y M and Liu Z 2008 Damage-freepolishing of monocrystalline silicon wafers without chemical additives *Scr. Mater.* **59** 1178–81